Source Illusion Devices for Flexural Lamb Waves Using Elastic Metasurfaces

Yongquan Liu,[1] Zixian Liang,[2] Fu Liu,[1] Owen Diba,[1] Alistair Lamb,[1] and Jensen Li[1,*]

[1]*School of Physics and Astronomy, University of Birmingham, Birmingham B15 2TT, United Kingdom*
[2]*College of Electronic Science and Technology, Shenzhen University, Shenzhen 518060, China*

Inspired by recent demonstrations of metasurfaces in achieving reduced versions of electromagnetic cloaks, we propose and experimentally demonstrate source illusion devices to manipulate flexural waves using metasurfaces. The approach is particularly useful for elastic waves due to the lack of form invariance in usual transformation methods. We demonstrate compact and simple-to-implement metasurfaces for shifting, transforming, and splitting a point source. The effects are measured to be broadband and robust against a change of source positions, with agreement from numerical simulations and the Huygens-Fresnel theory. The proposed method is potentially useful for applications such as nondestructive testing, high-resolution ultrasonography, and advanced signal modulation.

The ability to make objects invisible has captured our imagination since ancient times and has become reachable very recently due to the appearance of metamaterials [1] together with transformation optics [2–5]. A family of more general illusion effects has also been established based on the transformation approach. Either scattering [6,7] or source radiation [8] can be transformed to prescribed target patterns. Furthermore, the transformation approach has been extended to control acoustic waves [9–11] and heat flows [12–14]. Although some elastic cloaks have been studied and designed with approximations [15,16], the transformation method, together with elastic metamaterials [17–22], is nonuniversal to manipulate elastic waves, as the governing equation in elastodynamics (i.e., the Navier equation) cannot keep its form under a general coordinate transformation [23], unless further approximations [24] are applied or the proposed Willis media [25] can be realized and employed with a complex cross-coupling response. It makes the application of the transformation approach on elastic waves nontrivial and more generic illusion applications, which may use negative-index metamaterials with unavoidable loss and fabrication issues, very challenging.

On the other hand, the recently proposed metasurface [26–33], a kind of artificial sheet material with subwavelength-scaled patterns and thickness, can modulate wave fronts on demand through specific boundary conditions. The metasurface approach shows the simplicity in fabrication with a low-loss, compact form factor but without losing the extreme functionality of bulk metamaterials. It has already been demonstrated as an effective way to manipulate wave fronts in both optics and acoustics, including generating an anomalous refraction or reflection, arbitrary surface plasmon profiles, high-efficiency holograms [26–32], and even an ultrathin invisibility cloak [33,34], which is a simplified version of a carpet cloak originally using bulk metamaterials in the transformation approach [35]. Therefore, the extension of metasurfaces to

elastic waves is expected to be very effective to demonstrate nontrivial wave phenomena, which associate with richer physics [20–22] due to its more degrees of freedom than acoustic and electromagnetic counterparts and a wide range of potential applications in nondestructive testing, medical ultrasonography, and earthquake resistance in civil engineering [18,36–40]. Until very recently, Zhu and Semperlotti [41] have presented the first experimental demonstration of elastic metasurfaces to achieve the anomalous refraction of guided waves in solids, based on a "cross-polarization" conversion (from symmetric S_0 to antisymmetric A_0 mode) with a transmission efficiency around 18%, comparing to the theoretical maximum efficiency 25% in the case of electromagnetic waves [42,43]. A higher transmission efficiency, together with a suitable design framework, will be an enabling key to a much wider range of applications of elastic metasurfaces.

In this Letter, we develop a theoretical framework and experimental realization of source illusion devices using elastic metasurfaces. Our approach requires neither the fore-mentioned form invariance of elastodynamics nor bulk metamaterials with negative indices yet allows us to demonstrate a series of all-angle elastic illusion effects. Figure 1(a) shows a schematic diagram illustrating the design strategy. The target wave profile, living in the virtual space, is described by its phase profile $\phi_{\text{tar}}(x, y)$ [left-hand side of Fig. 1(a)]. At the moment, we neglect the contribution of the amplitude profile for simplicity. Suppose that we have an original source, with a wave field characterized by its phase $\phi_{\text{ori}}(x, y)$, and a ring-type metasurface with the phase discontinuity of $\phi_{\text{tar}} - \phi_{\text{ori}}$, being evaluated at the location of the metasurface, will turn this original incident field into an arbitrary target profile [right-hand side of Fig. 1(a)]. A photograph of a metasurface sample is shown in Fig. 2(a) as well. By doing this, an observer outside the metasurface (the black dashed circle) finds the same target field pattern in the physical space as
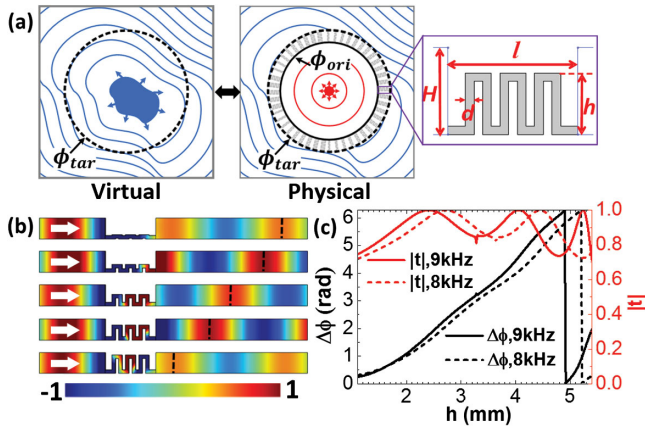
FIG. 1. (a) Schematic of making illusions using metasurfaces. The target profile is achieved by the combination of the original profile and the phase discontinuity caused by metasurface. The unit cell is enlarged and dimensioned in the right part. (b) Simulated out-of-plane displacement field produced by different heights h of three-turn unit cells. Crests of transmitted waves (black dashed lines) shift left with the increase of h, inferring the increase of phase discontinuity. (c) Phase discontinuity $\Delta\phi$ (black lines) and amplitude of transmitted waves $|t|$ (red lines) as a function of h. Dashed and solid lines correspond to the results at 8 and 9 kHz, respectively.

FIG. 2. (a) Source shifter. (b) Expected profile of the source shifter. The physical point source at the center (black circular point with arrows) is shifted horizontally to the left by $\Delta S = 25$ mm. Crests of the target pattern are plotted as gray lines. (c) The normalized amplitude of the experimentally measured A_0 wave field at 12 kHz. (d) Experimentally measured wave field at 10 kHz. (e) Experimentally measured wave field at 12 kHz; the source is placed at $(25, 0)$ mm. In (c)–(e), crests of the theoretical patterns are plotted based on the Huygens-Fresnel theory as dashed gray lines accordingly.

designed in the virtual space. Next, the phase discontinuity can be achieved by a particular metasurface design, which should cover an entire phase change of 2π with a preferably unit transmission amplitude. A previous design [41] utilized resonant unit cells with mode conversion from S_0 mode to A_0 mode to achieve a full coverage of 2π, which leads to low power of transmitted waves. In light of this, we design elastic metasurfaces with negligible mode conversion [44,28–30] based on the zigzag structures. Figure 1(a) shows the schematic of our design to realize the phase discontinuity. Each unit cell of the ring-type metasurface consists of a curved thin bar with identical width d and height of turns h. It modulates the propagation phase of the guided asymmetric Lamb wave (A_0 mode) within a 3-mm-thick acrylic plate.

To illustrate its working mechanism, Fig. 1(b) shows simulations of the out-of-plane displacement field, which corresponds to the A_0 mode Lamb wave, produced by different heights h of three-turn unit cells. The wave is restricted to propagate along a zigzag path shaped by the unit cell. By increasing the height of turns h, we can increase the phase discontinuity $\Delta\phi$ of transmitted waves due to the increase of the total path length. In consequence, the crests of the wave profiles (dashed black lines) in the transmission side gradually shift to the left. Figure 1(c) describes the phase discontinuity $\Delta\phi$ (black lines) and the amplitude of transmitted A_0 waves $|t|$ (red lines) of unit cells versus h with the chosen geometric parameters of $d = 1$ mm, $l = 15$ mm, and $H = 5.89$ mm at 8 and 9 kHz. It is worth noting that the average value of $|t|$ is over 0.85

with respect to the incident A_0 wave, corresponding to a transmission power above 72%. The high transmission of power into the curved thin bar is due to the existence of the evanescent mode on the interface to have better impedance matching, in contrary to the scalar acoustic case [45]. It infers that this unit cell can redirect the wave front without significant reflected waves. It enables the illusion effects demonstrated in this work. Moreover, the phase discontinuity $\Delta\phi$ can keep its monotonic trend against h and a full coverage of 2π with a broadband range of frequency (8 and 9 kHz as examples).

As the first example, an illusion device for shifting the position of a wave source virtually, termed as a source shifter, is constructed, with its effect schematically shown in Fig. 2(b). Previous illusion optical devices [8] are composed of bulk materials with inhomogeneous parameters, resulting from the transformation approach. Here we achieve the illusion effect using a ring-shape metasurface to shift the source horizontally by a distance ΔS to the left. Suppose we take a special case where a physical source at origin $(0,0)$ is shifted to a virtual one at $(-\Delta S, 0)$. The shifting action of the metasurface, of radius R, has to satisfy phase discontinuity as a function of azimuthal angle θ, given by

$$\phi_{\text{tar}} - \phi_{\text{ori}} = \frac{2\pi}{\lambda}(R' - R), \qquad (1)$$

where $R' = \sqrt{(R\cos\theta + \Delta S)^2 + (R\sin\theta)^2}$ and λ is the working wavelength in the acrylic plate. Here, we set $R = 57$ mm, $\Delta S = 25$ mm, and $\lambda = 26.0$ mm (at 12 kHz). Then the metasurface with 48 unit cells possessing the required phase change is designed and fabricated. Detailed geometric parameters of the unit cells (with photographs) are provided in Ref. [45]. The out-of-plane velocity field is measured by a laser scanning vibrometer (Polytec PSV-400). Detailed experimental procedures are provided in Ref. [45]. Figure 2(c) shows the full-field experimental results. Inside the ring, it is the circular wave front expected from the point source before the transformation. Circular wave fronts are also measured outside the metasurface, centered at about 25.2 mm on the left of the exciting point source, which is very close to the target value 25 mm. The ripples can be improved by using smaller unit cells or optimizing the structural units to reduce multiple reflections in the core of metasurface [45].

To illustrate the robustness of our metasurface, Fig. 2(d) shows the normalized wave field at another frequency, 10 kHz. Apart from the change of wavelength from 26.0 to 28.7 mm, a similar wave pattern, wave fronts with a common center, is still found to match the target one (presented as dashed gray lines), with an illusion about shifting the point source horizontally to the left by 27.5 mm. More interestingly, if we place the source at some other locations, e.g., $(x_0, 0)$, the wave fronts outside are still found to have the shifted common center at around $(x_0 - \Delta S, 0)$. It works well from $x_0 = -20$ to 30 mm, with a correlation coefficient larger than 0.55, in measuring the similarity between the target and resultant pattern [45]. Figure 2(e) presents the measured wave pattern for a particular case, $x_0 = 25$ mm, where the common center is found at the origin. Based on the Huygens-Fresnel diffraction theory, the wave profile outside the metasurface can be calculated, with crests plotted as dashed gray lines in Fig. 2(e), coinciding with the experimental result. The resultant wave front has a small deviation from circular shape near the metasurface, with a detailed analysis given in Ref. [45]. The associated numerical simulations of the experimental configurations in Fig. 2 are provided in more detail in Ref. [45].

Our elastic metasurfaces can also be used to transform a point source to a prescribed target wave front. Here we impart an additional angular momentum [26] to the point source as an intuitive example. The observer outside perceives it as a point source with a spiral wave front. In this case, the phase discontinuity should be simply as

$$\phi_{\text{tar}} - \phi_{\text{ori}} = L\theta + \phi_0 \qquad (2)$$

with L being the additional angular momentum (integer) and ϕ_0 being an arbitrary constant. We set $L = 6$,
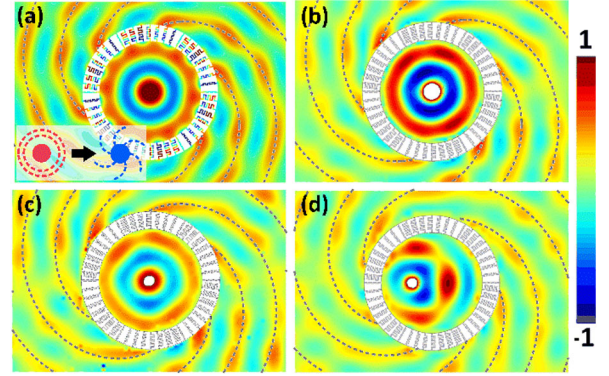
FIG. 3.   (a) Full wave simulation results of an illusion metasurface imparting an angular momentum of $L = 6$ to a point source, with the illusion effect schematically shown in the inset. (b) Experimentally measured A_0 wave field at 8 kHz. The point source is placed at the center. (c) Experimentally tested wave field at 10 kHz. (d) Experimentally measured wave field at 8 kHz; the source is placed at $(-15, 0)$ mm. In all subplots, crests of wave profiles, from Eq. (3), are plotted as dashed lines accordingly.

$R = 60$ mm, and the operating frequency at 8 kHz; the metasurface can be designed and fabricated with a similar procedure [45]. Figure 3(a) shows the full wave simulations of the A_0 mode wave field excited by a point source at the center, and Fig. 3(b) illustrates the corresponding experimental results. In the external region of the metasurface, the cylindrical wave shapes into a spiral with evenly distributed six branches. All branches are centered at the original point. It is noted that the number of branches equals the additional momentum L; equivalently, the wave undergoes a phase change of $2\pi L$ for walking around one cycle in the azimuthal direction. For comparison, we also plot the crests of the theoretical pattern as dashed lines in Figs. 3(a) and 3(b), which coincides with both the numerical and experimental results.

The designed metasurface also works with a variation of the working frequency and source position. For instance, if we change the experimental frequency to 10 kHz for the same designed metasurface [Fig. 3(c)], we can still achieve a similar six-branched spiral wave field, except the wavelength is changed from 32.4 to 28.7 mm. In another case, we place the source at $(-15, 0)$ mm instead of the origin; the measured wave pattern is shown in Fig. 3(d). Again, a spiral wave front with six branches, indicating $L = 6$, is found. The wave field with a generic source position can be explained by the Huygens-Fresnel principle, with the phase outside the metasurface being approximated as

$$\phi_{\text{out}}(x, y) = L\theta + k(s_1 + s_2) + \phi_0, \qquad (3)$$

having the same target angular momentum L, where $s_2 = \sqrt{(R\cos\theta - x_0)^2 + (R\sin\theta - y_0)^2}$ and (x_0, y_0) is the position

of the actual point source, $s_1 = |(x+iy)e^{-i\theta} - R| \cong \sqrt{x^2 + y^2} - R$. Crests of the theoretical profile predicted by Eq. (3) are plotted as dashed gray lines in Fig. 3(d), matching the experimental results.

It should be noted that the two demonstrated metasurfaces make illusions of a single point source. In both cases, the amplitude of the wave pattern on the metasurface boundary changes only slightly. Hence, as a prerequisite of keeping a high value of the transmittance, we just need to tune the phases of metasurfaces. We need only to utilize three-turned unit cells for the design of the above two metasurfaces. As a further step, we now demonstrate the case with a changing wave amplitude on the metasurface boundary as our final example. As shown in Fig. 4(a), a source splitter is designed to mimic a wave pattern of two sources with opposite phases from a single physical point source at origin. The two virtual sources are set at positions $(0, \pm a) = (0, \pm 20)$ mm, respectively, and the designed frequency is 8 kHz. Then the metasurface has to satisfy a phase discontinuity of

$$\mathrm{Arg}[H_0^{(1)}(kr_1) - H_0^{(1)}(kr_2)] - \mathrm{Arg}[H_0^{(1)}(kr)],$$

where $r_{1,2} = \sqrt{(R\cos\theta)^2 + (R\sin\theta \mp a)^2}$ and $H_0^{(1)}(\cdot)$ is the zeroth-order Hankel function of the first kind. However, due to the interference of the two target virtual sources, the amplitude also varies greatly on the metasurface boundary. In this case, we need to have unit cells possessing adequate phase shifts (0 to 2π) and transmittances (0 to 1) simultaneously. By changing the width d and the number of turns to incorporate resonance, a very low to high transmission amplitude can be achieved. As an example, Fig. 4(b) shows
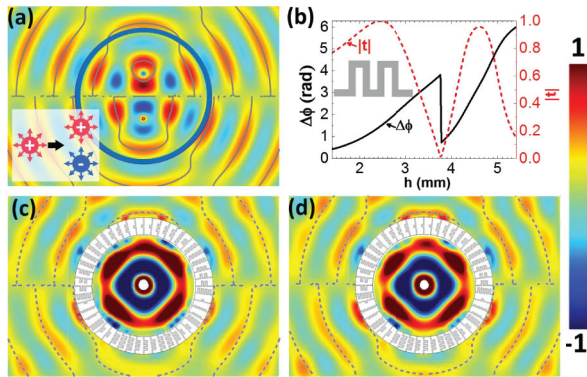
FIG. 4. Source splitter metasurface. (a) The target profile from two point sources at $(0, \pm 20)$ mm with opposite phases at 8 kHz, with the illusion effect schematically shown in the inset. (b) The phase discontinuity $\Delta\phi$ (black line) and the amplitude of transmitted waves $|t|$ (dashed red line) of a two-turn unit cell with $l = 15$ mm and $d = 1$ mm, as a function of h at 8 kHz. (c) Experimentally measured A_0 wave field at 8 kHz. (d) Experimentally tested pattern at 8.2 kHz. In subplots (a), (c), and (d), crests of the target pattern are plotted as gray lines.

the phase discontinuity $\Delta\phi$ (black line) and amplitude of the transmitted wave $|t|$ (dashed red line) of a two-turn unit cell with $l = 15$ mm and $d = 1$ mm, as a function of h at 8 kHz. The amplitude of transmitted waves can be as low as zero when $h = 3.76$ mm and can be freely tuned due to a twisting mode resonance; see Supplemental Material [45]. We note that mode conversions to SH_0 and S_0 modes are avoided due to symmetry of the designed structure [45]. Based on this mechanism, six types of unit cells with different widths d and different numbers of turns are utilized to construct this metasurface. Details of each unit cell are provided in Ref. [45]. Figure 4(c) presents the experimentally measured A_0 wave field at 8 kHz. The wave is excited by a point source at the origin, and an interference pattern is observed outside the metasurface. Because of the low transmittance of some unit cells, the amplitude inside the metasurface is much larger than that outside. The theoretical wave fronts at zero phase are plotted as dashed lines outside the metasurface for comparison. It is worth noting that the amplitude on the x axis is nearly zero as an indication of amplitude control to obtain the target interference pattern, such that waves propagating in the upper and lower planes can have a π phase lag with each other. Although resonance is employed, there is still an acceptable bandwidth for operation [45], e.g., at 8.2 kHz [Fig. 4(d)], except the wavelength of the circular wave front is changed from 32.4 to 31.9 mm.

The illusion devices described above are just a few examples; more elaborate illusion effects are expected in future works, such as combining the power of two or more sources for omnidirectional radiation or making an arbitrary scatterer appear as a very different one originally in the electromagnetic and acoustic cases [6,8]. Therefore, a variety of promising applications are expected based on the proposed strategies. For example, the source transformer imparting an additional angular momentum provides an additional degree of freedom for signal modulation [26], and the source splitter can be used as compact devices with phased array sources for nondestructive testing and ultrasonic imaging [49]. It is worth noting that bulk metamaterials with extreme or negative refractive indices are often required for illusion devices from the transformation approach. Nevertheless, our metasurfaces are quite compact, with a thickness less than half of the wavelength.

The source shifter and source transformer are designed without using the resonant mechanism. Thus, they are able to work broadband with high power output. For the source shifter, we have achieved a correlation coefficient between the target and experimentally realized pattern over 0.7 (3 dB drop in amplitude from the ideal value of 1) from 10 to 13.5 kHz. The source transformer works over a frequency range of 6 to 10 kHz with the same 3 dB drop and, thus, with a bandwidth more than 50% of the central frequency. Moreover, when we change the position of the source, the corresponding target phase ϕ_{tar} and the original phase ϕ_{ori} are found to have approximately the same difference so

that the same devices are still valid, as illustrated in Figs. 2(e) and 3(d), as generic illusion effects. For example, as shown numerically in Ref. [45], the source transformer can still preserve a six-branched spiral pattern when setting the source at (10, 10) mm.

In summary, we have developed a generic framework to make source illusions for A_0 mode Lamb waves using compact elastic metasurfaces. As examples, we designed and experimentally demonstrated three all-direction illusion devices to shift the position of a point source, to impart additional angular momentum, and to split a point source into two, respectively. The demonstrated illusion effects are robust against a change of working frequency and position of the source. Without requiring form invariance of the governing equation in elastodynamics to achieve illusion effects, the proposed approach paves the way to more "transformation-approach"-type applications to control elastic waves.

---

*Corresponding author.
j.li@bham.ac.uk

[1] D. R. Smith, J. B. Pendry, and M. C. Wiltshire, Science **305**, 788 (2004).

[2] U. Leonhardt, Science **312**, 1777 (2006).

[3] J. B. Pendry, D. Schurig, and D. R. Smith, Science **312**, 1780 (2006).

[4] D. Schurig, J. J. Mock, B. J. Justice, S. A. Cummer, J. B. Pendry, A. F. Starr, and D. R. Smith, Science **314**, 977 (2006).

[5] H. Chen, C. T. Chan, and P. Sheng, Nat. Mater. **9**, 387 (2010).

[6] Y. Lai, J. Ng, H. Y. Chen, D. Z. Han, J. J. Xiao, Z. Q. Zhang, and C. T. Chan, Phys. Rev. Lett. **102**, 253902 (2009).

[7] C. Li, X. Meng, X. Liu, F. Li, G. Fang, H. Chen, and C. T. Chan, Phys. Rev. Lett. **105**, 233906 (2010).

[8] H. Chen, Y. Xu, H. Li, and T. Tyc, New J. Phys. **15**, 093034 (2013).

[9] S. Zhang, C. Xia, and N. Fang, Phys. Rev. Lett. **106**, 024301 (2011).

[10] B. I. Popa, L. Zigoneanu, and S. A. Cummer, Phys. Rev. Lett. **106**, 253901 (2011).

[11] L. Sanchis, V. M. García-Chocano, R. Llopis-Pontiveros, A. Climente, J. Martínez-Pastor, F. Cervera, and J. Sánchez-Dehesa, Phys. Rev. Lett. **110**, 124301 (2013).

[12] R. Schittny, M. Kadic, S. Guenneau, and M. Wegener, Phys. Rev. Lett. **110**, 195901 (2013).

[13] H. Xu, X. Shi, F. Gao, H. Sun, and B. Zhang, Phys. Rev. Lett. **112**, 054301 (2014).

[14] T. Han, X. Bai, D. Gao, J. T. L. Thong, B. Li, and C. W. Qiu, Phys. Rev. Lett. **112**, 054302 (2014).

[15] M. Farhat, S. Guenneau, and S. Enoch, Phys. Rev. Lett. **103**, 024301 (2009).

[16] N. Stenger, M. Wilhelm, and M. Wegener, Phys. Rev. Lett. **108**, 014301 (2012).

[17] Z. Liu et al., Science **289**, 1734 (2000).

[18] R. Zhu, X. N. Liu, G. K. Hu, C. T. Sun, and G. L. Huang, Nat. Commun. **5**, 5510 (2014).

[19] J. Lu, C. Qiu, M. Ke, and Z. Liu, Phys. Rev. Lett. **116**, 093901 (2016).

[20] S. Y. Yu, X.-C. Sun, X. Ni, Q. Wang, X.-J. Yan, C. He, X.-P. Liu, L. Feng, M.-H. Lu, and Y.-F. Chen, Nat. Mater. **15**, 1243 (2016).

[21] J. H. Oh, Y. E. Kwon, H. J. Lee, and Y. Y. Kim, Sci. Rep. **6**, 23630 (2016).

[22] G. Ma, C. Fu, G. Wang, P. del Hougne, J. Christensen, Y. Lai, and P. Sheng, Nat. Commun. **7**, 13536 (2016).

[23] G. W. Milton, M. Briane, and J. R. Willis, New J. Phys. **8**, 248 (2006).

[24] J. Hu, Z. Chang, and G. Hu, Phys. Rev. B **84**, 201101 (2011).

[25] G. W. Milton and J. R. Willis, Proc. R. Soc. A **463**, 855 (2007).

[26] N. Yu, P. Genevet, M. A. Kats, F. Aieta, J.-P. Tetienne, F. Capasso, and Z. Gaburro, Science **334**, 333 (2011).

[27] X. Ni, N. K. Emani, A. V. Kildishev, A. Boltasseva, and V. M. Shalaev, Science **335**, 427 (2012).

[28] Y. Cheng, C. Zhou, B. G. Yuan, D. J. Wu, Q. Wei, and X. J. Liu, Nat. Mater. **14**, 1013 (2015).

[29] Y. Xie, W. Wang, H. Chen, A. Konneker, B. I. Popa, and S. A. Cummer, Nat. Commun. **5**, 5553 (2014).

[30] Y. Li, X. Jiang, R. Q. Li, B. Liang, X. Y. Zou, L. L. Yin, and J. C. Cheng, Phys. Rev. Applied **2**, 064002 (2014).

[31] S. Sun, Q. He, S. Xiao, Q. Xu, X. Li, and L. Zhou, Nat. Mater. **11**, 426 (2012).

[32] G. Zheng, H. Mühlenbernd, M. Kenney, G. Li, T. Zentgraf, and S. Zhang, Nat. Nanotechnol. **10**, 308 (2015).

[33] X. Ni, Z. J. Wong, M. Mrejen, Y. Wang, and X. Zhang, Science **349**, 1310 (2015).

[34] B. Orazbayev, N. Mohammadi Estakhri, A. Alù, and M. Beruete, Adv. Opt. Mater. **5**, 1600606 (2017).

[35] J. Li and J. B. Pendry, Phys. Rev. Lett. **101**, 203901 (2008).

[36] C. T. Ng and M. Veidt, Smart Mater. Struct. **18**, 074006 (2009).

[37] A. Sukhovich, B. Merheb, K. Muralidharan, J. O. Vasseur, Y. Pennec, P. A. Deymier, and J. H. Page, Phys. Rev. Lett. **102**, 154301 (2009).

[38] J. Li, L. Fok, X. Yin, G. Bartal, and X. Zhang, Nat. Mater. **8**, 931 (2009).

[39] J. Zhu, J. Christensen, J. Jung, L. Martin-Moreno, X. Yin, L. Fok, X. Zhang, and F. J. Garcia-Vidal, Nat. Phys. **7**, 52 (2011).

[40] S. Brulé, E. H. Javelaud, S. Enoch, and S. Guenneau, Phys. Rev. Lett. **112**, 133901 (2014).

[41] H. Zhu and F. Semperlotti, Phys. Rev. Lett. **117**, 034302 (2016).

[42] F. Monticone, N. M. Estakhri, and A. Alù, Phys. Rev. Lett. **110**, 203903 (2013).

[43] X. Ding, F. Monticone, K. Zhang, L. Zhang, D. Gao, S. N. Burokur, A. de Lustrac, Q. Wu, C.-W. Qiu, and A. Alù, Adv. Mater. **27**, 1195 (2015).

[44] Z. Liang and J. Li, Phys. Rev. Lett. **108**, 114301 (2012).

[45] See Supplemental Material at http://link.aps.org/
supplemental/10.1103/PhysRevLett.119.034301 for the ex-
perimental setup, detailed results, and analysis, which
includes Refs. [46–48].

[46] M. C. Cross and R. Lifshitz, Phys. Rev. B **64**, 085324
(2001).

[47] J. D. Jackson, *Classical Electrodynamics* (John Wiley &
Sons, New York, 1999), 3rd ed.

[48] Z. Qiu, J. Yue, X. Wang, and S. Yue, PLoS One **11**,
e0148823 (2016).

[49] M. Senesi, B. Xu, and M. Ruzzene, Smart Mater. Struct. **19**,
055026 (2010).